

Electron emission induced by keV protons from tungsten surface at different temperatures

Li-Xia Zeng(曾利霞), Xian-Ming Zhou(周贤明), Rui Cheng(程锐), Yu Liu(柳钰), Xiao-An Zhang(张小安), and Zhong-Feng Xu(徐忠锋)

Citation: Chin. Phys. B, 2022, 31 (**7**): 073202. DOI: 10.1088/1674-1056/ac632f
Journal homepage: http://cpb.iphy.ac.cn; http://iopscience.iop.org/cpb

What follows is a list of articles you may be interested in

Nd *L*-shell x-ray emission induced by light ions

Xian-Ming Zhou(周贤明), Jing Wei(尉静), Rui Cheng(程锐), Yan-Hong Chen(陈燕红),Ce-Xiang Mei(梅策香), Li-Xia Zeng(曾利霞), Yu Liu(柳钰), Yan-Ning Zhang(张艳宁), Chang-Hui Liang(梁昌慧), Yong-Tao Zhao(赵永涛), and Xiao-An Zhang(张小安)

Chin. Phys. B, 2022, 31 (**6**): 063204. DOI: 10.1088/1674-1056/ac4488

Relative phase-dependent two-electron emission dynamics with two-color circularly polarized laser fields

Tong-Tong Xu(徐彤彤), Lian-Lian Zhang(张莲莲), Zhao Jin(金钊), Wei-Jiang Gong(公卫江)

Chin. Phys. B, 2020, 29 (**9**): 093202. DOI: 10.1088/1674-1056/ab928c

Interpulse interference of electron emission from an atom irradiated by sinusoidally phase-modulated pulse

Hai-Ying Yuan(袁海颖), Fu-Ming Guo(郭福明), Di-Yu Zhang(张頔玉), Jun Wang(王俊), Ji-Gen Chen(陈基根), Yu-Jun Yang(杨玉军)

Chin. Phys. B, 2018, 27 (**10**): 103201. DOI: 10.1088/1674-1056/27/10/103201

Simultaneous study of the lower order harmonic and photoelectron emission from an atom in intense laser pulse

Yan Yan(闫妍), Fu-Ming Guo(郭福明), Jun Wang(王俊), Ji-Gen Chen(陈基根), Yu-Jun Yang(杨玉军)

Chin. Phys. B, 2018, 27 (**8**): 083202. DOI: 10.1088/1674-1056/27/8/083202

Significant discrepancy between the ionization time for parallel and anti-parallel electron emission in sequential double ionization

Wang Xiao-Shan, Du Hong-Chuan, Luo Lao-Yong, Hu Bi-Tao

Chin. Phys. B, 2013, 22 (**9**): 093201. DOI: 10.1088/1674-1056/22/9/093201

Electron emission induced by keV protons from tungsten surface at different temperatures

Li-Xia Zeng(曾利霞)[1,2,†], Xian-Ming Zhou(周贤明)[1,2], Rui Cheng(程锐)[3], Yu Liu(柳钰)[1], Xiao-An Zhang(张小安)[1,3], and Zhong-Feng Xu(徐忠锋)[2,3,‡]

[1] *Ion Beam and Optical Physical Laboratory, Xianyang Normal University, Xianyang* 712000, *China*
[2] *Institute of Science and Technology for Laser and Particle Beams, Xi'an Jiaotong University, Xi'an* 710049, *China*
[3] *Institute of Modern Physics, Chinese Academy of Science, Lanzhou* 730000, *China*

(Received 26 November 2021; revised manuscript received 17 February 2022; accepted manuscript online 1 April 2022)

The electron emission yield is measured from the tungsten surface bombarded by the protons in an energy range of 50 keV–250 keV at different temperatures. In our experimental results, the total electron emission yield, which contains mainly the kinetic electron emission yield, has a very similar change trend to the electronic stopping power. At the same time, it is found that the ratio of total electron emission yield to electronic stopping power becomes smaller as the incident ion energy increases. The experimental result is explained by the ionization competition mechanism between electrons in different shells of the target atom. The explanation is verified by the opposite trends to the incident energy between the ionization cross section of M and outer shells.

Keywords: electron emission, x-ray, electronic stopping power, work function

PACS: 32.80.Aa, 32.30.Rj, 34.80.Dp, 79.20.Rf **DOI:** 10.1088/1674-1056/ac632f

1. Introduction

The interactions of charged ions and strong radiation with solid targets have been widely concerned in recent years. The underlying physical processes are very important for not only basic physics, but also technical applications, such as material surface modification, x-ray source equipment, radiation physics, plasma–wall interactions, and material surface analysis as well.[1–8] When a charged ion impacts solid target, it will deposit most of its potential energy into several atomic layers through the process of neutralization and de-excitation within femtoseconds.[3] At the same time, through inelastic collisions, the kinetic energy of the ion can be transferred into valence electrons or inner-shell electrons, resulting in the shell ionization. In this collision process, electrons and x-rays will be emitted with the ionization of incident ions and the decay of vacancies in the inner shell.[9,10] Therefore, electron emission and x-rays provide reliable information for studying particle properties and mechanism of ion–atom collision process.

The electron emission process is usually described by the average number of electrons emitted each incident ion, that is, the electron emission yield γ. As is well known, the electron emission yield is related to the charge state, velocity, incident energy, atomic number and incident angle of incident ions, and so on.[4–8] We have also studied the influence of state of charge of incident ion, recoil atoms, and target temperature on the electron emission yield γ.[11–13] Electron emission caused by highly charged ions (HCIs) is usually divided into two different mechanisms, one is the potential emission (PE) process and the other is the kinetic emission (KE) process.[14,15] It is generally believed that electron emission is closely related to the deposition of electron excitation near the target surface. The kinetic electron emission (KEE) yield is believed to be related to the electronic stopping power of slow light ions. Energy deposition depends on the velocity and charge state of incident ions. The proportion of energy, which is used to generate electron emission, varies with the incident energy.

The characteristic x-rays, which are produced by ion-solid interactions, mainly come from the de-excitation of hollow atoms in the low-energy region, and the attenuation of vacancy in the inner shell, caused by direct ionization during the bombardment of high-energy projectiles. The x-rays have been extensively investigated experimentally, and many theories have been proposed to successfully describe this process. Common theories include the classical barrier-crossing model for the evolution of incident ions around the surface, the binary encounter approximation (BEA), the plane-wave Born shell approximation of electron ionization (PWBA) and the energy-loss Coulomb-repulsive perturbation steady-state relativity (ECPSSR) for the ionization of the shell electrons.[16–18] A lot of researches have been done to study electron emission[1–3,11–13] and x-rays.[4,19] However, there are few studies on these two phenomena at the same time.[20] We have not found the researches about the electron emission from tungsten surface at different temperatures. Here in this work, we will explore the correlation between the two phenomena. Our recent experimental results on the kinetic elec-

[†]Corresponding author. E-mail: zenglixia1982@126.com
[‡]Corresponding author. E-mail: zhfxu@mail.xjtu.edu.cn

© 2022 Chinese Physical Society and IOP Publishing Ltd

tron and x-ray emission induced by keV protons from tungsten surface at different temperatures will be shown.

In this paper, we present the experimental results about the electron emission yield from tungsten surface bombarded by protons in an energy range of 50 keV–250 keV at different target temperatures. The mechanism of electron emission is investigated and verified experimentally and theoretically. Our experimental results will be helpful in studying the electron and x-ray emission of tungsten, which has been selected and used as the first wall material of the International Thermonuclear Experimental Reactor (ITER).

2. Experimental setup

The experiment was carried out on the 320-kV electron cyclotron resonance ion source (ECRIS) platform of the Institute of Modern Physics, Chinese Academy of Sciences (IMP, CAS) in Lanzhou.[21] Many experiments on the study of highly charged ions incident on solid surfaces have been carried out on this platform.[11–13,20–22] Our experimental method can be seen elsewhere.[11–13] In the experiment, our experimental device was in an ultrahigh vacuum (UHV) target chamber (10^{-9} mbar–10^{-10} mbar, 1 bar = 10^5 Pa). Figure 1 shows the experimental setup for electron emission yield measurement. It mainly consisted of four parts, namely, beam collimator, rejection aperture with a diameter of 3 mm, ultrahigh vacuum heater and cage. The beam collimator was used to prevent incident ions from hitting the rejection aperture directly and was 3 mm in diameter. A rejection electrode with a potential of −100 V was located in front of the cage. In this way, electrons were prevented from escaping and the electron collection efficiency was improved. The cage surrounded the target, and a voltage of ±100 V was applied to the cage, for collecting or suppressing the electrons emitted from the target. The cage had 5 mm in aperture diameter serving as an ion beam entrance and collimated the incident ion beam before it reached the target surface. We collimated the beam by monitoring the current on the cage and the target. When the current on the cage was zero and the target current reached a maximum value, it was the best position. The sample in this experiment was solid polycrystalline tungsten with a purity of 99.99%. The sample was first mechanically polished, then washed in acetone and ethanol, and finally cleaned by heating in UHV. We used the UHV heater, which was produced by Heat Wave Labs, to control the target temperature. An insulating sheet was placed between the target and the heater. The incident protons were generated and extracted from a 14.5-GHz electron cyclotron resonance (ECR) ion source. As a result of being focused and collimated, the diameter of these incident proton beams was 3 mm. The current on the target was measured by Keithley 6485 picoammeter and integrated, with a time integration constant being about 25 s.

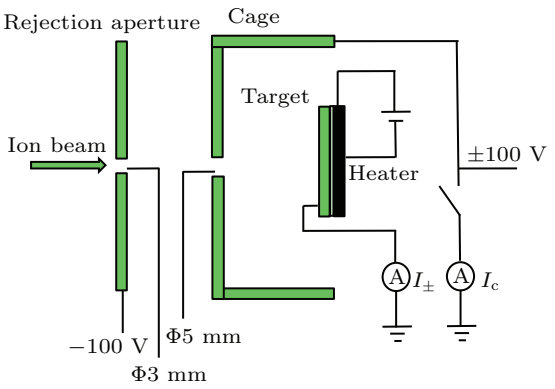


Fig. 1. Schematic diagram of experimental setup used for measuring total electron yield.

The total electron emission yield γ is given as[11–13]

$$\gamma = q\frac{I_+ - I_-}{I_-}, \tag{1}$$

where q is the state of charge of the incident ion, I_+ and I_- are the target currents for ±100 V of voltages applied to the cage.

The emitted x-rays were measured by a silicon drift detector (SDD), and its effective detection area was 7 mm^2. A window of 12.5-μm beryllium was placed directly in front of the detector. The distance between the SDD and the target surface was 80 mm, which was 135° with respect to the direction of incident ion beam. When the gain was set to be 100, the effective energy range of this detector was 0.5 keV–14.3 keV. The energy resolution of 5.9 keV was approximately 136 eV, when the peak time was 9.6 s. We used standard radioactive sources ^{55}Fe and ^{241}Am to calibrate and determined the efficiency through transmission measurement.

3. Results and discussion

It can be found from Fig. 2 that the incident ion beam current is very stable and almost constant in the experiment. The electrons escaping from the target surface are suppressed by applying a −100-V voltage to the cage, and they are collected under the opposite voltage. Our previous study shows that the total electron emission yield is independent of ion current,[13,21] so we do not repeat the measurements here.

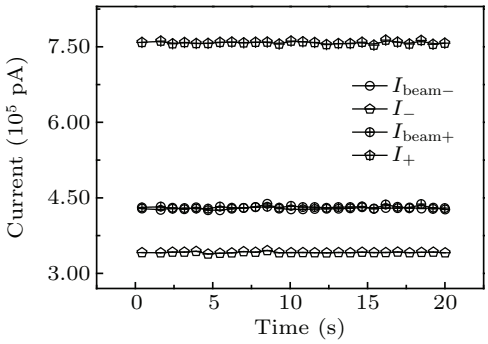


Fig. 2. Typical time-dependent currents recorded for electron emission induced by 200-keV protons at target temperature of about 286 °C, with I_{beam} denoting current of incident beam.

Total electron yields from tungsten surface induced by protons as a function of incident energy at different target temperatures are shown in Fig. 3. The error bars shown in the figure are statistical errors. Our experimental results of the total electron emission yield (γ) are consistent with the results of γ for Ewing's polycrystalline target within the error range.[20,23] The total electron yields have similar dependence on the proton energy at different target temperatures. It can be found from Fig. 4 that the experimental curves have a similar change trend with the stopping power, calculated using SRIM.[24] Specifically, they start to increase from the low energy end, reach their maximum values at about 100 keV, and finally decrease with kinetic energy increasing.

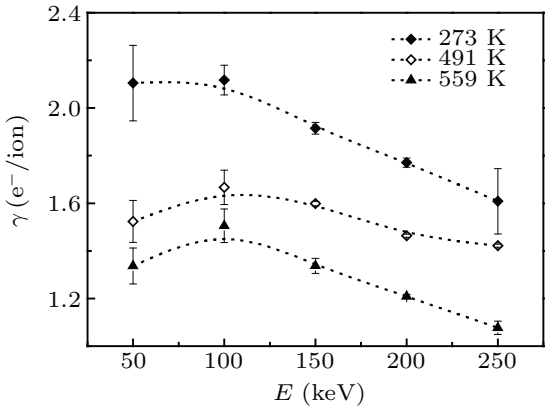


Fig. 3. Electron yields from tungsten surface induced by protons as a function of incident energy at different target temperatures.

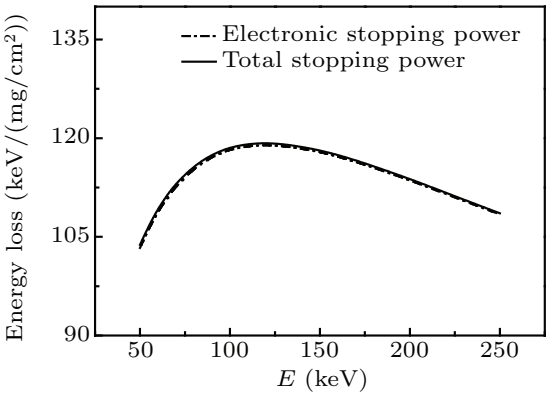


Fig. 4. Electronic stopping power S_e and total stopping power S_t as a function of projectile energy for 50 keV–250 keV protons impacting solid tungsten target, calculated by SRIM.

Because of their kinetic and potential energy and high ionization state, highly charged ions become effective carriers of energy. As mentioned earlier, electron emission processes caused by highly charged ions are usually divided into two types, namely the potential emission (PE) process and the kinetic emission (KE) process.[14,15] Therefore, the total electron emission yield γ can be divided into the kinetic electron yield γ_{KE} and the potential electron yield γ_{PE}. For the potential emission process, the potential energy carried by the incident ion needs to be greater than twice the work function W_ϕ of the solid target surface.

Here, the first ionization energy E_{pot} for proton is 13.6 eV, more than twice the work function W_ϕ for the polycrystalline tungsten, which is 4.55 eV.[25] The maximum possible number of electrons caused by potential energy deposition can be given by[26]

$$n_{max} = E_{pot}/2W_\phi. \tag{2}$$

Here, n_{max} is approximately equal to 1.51, which is nearly equal to the total yield at 50-keV incident energy, and is greater than the total yield at 250-keV incident energy when the target temperature is 491 K. However, this maximum cannot be achieved, and only a small part of the potential energy is used for potential electron emission, because part of the electrons excited by the potential energy cannot escape from the target surface.[26,27] In fact, owing to the incomplete neutralization of incident ions, the potential energy cannot be fully used to excite electrons. The classical γ_{PE} is given by[27]

$$\gamma_{PE} \approx \frac{0.2}{E_F}(0.8E_{pot} - 2W_\phi). \tag{3}$$

Here, E_F is the Fermi energy of the solid target. Using Eq. (3), we can estimate that γ_{PE} is approximately equal to 0.08 in our experiment. It is only a very small part of the total yield, which is negligible compared with γ_{KE}. Therefore, the electron emission yield γ in our experiment results mainly from the KE process, that is to say, the total electron yield can be given as

$$\gamma \approx \gamma_{KE}. \tag{4}$$

Kinetic energy electrons are caused mainly by directly ionizing the valence electrons and inner shell electrons, and the secondary ionization of outer shell electrons due to Auger transition. Direct ionization is directly related to the ionization cross sections of electrons in different shells. The factors that can affect the secondary ionization are inner shell ionization, the probability of Auger transition and the secondary ionization cross section. Obviously, this is smaller than the ionization cross section of the inner shell electrons. The studies have shown that inner shell ionization plays a negligible role in the KE process of low-energy light ion incidence.[18] This means that the contribution of the inner shell excitation and the Auger decay of the subsequence can be ignored. From this we can know that the escape of excited valence electrons is the main factor in our measured kinetic electron yield. And γ_{KE} is often calculated from

$$\gamma_{KE} = \frac{BS_e}{\sin(\Psi)}, \tag{5}$$

where S_e is the electronic stopping power, Ψ is the incident angle of the incident ion, and B can be regarded as a constant, which decreases slightly as the kinetic energy and atomic number of the incident ion increase.[28,29] In our measurement, the

ion beam is incident perpendicular to the target surface, therefore, $\sin(\Psi) = 1$, so

$$\gamma_{(\mathrm{Se})} = BS_{\mathrm{e}}. \tag{6}$$

Figure 5 shows the ratio of total electron emission yield γ to electronic stopping power S_{e} as a function of the incident energy. Here γ is the experimental value we measured, and S_{e} is calculated using SRIM as shown in Fig. 4. We can find from Fig. 5 that the ratio is not a fixed value, it will decrease slightly as the proton energy increases. Here, we will explain the down trend of B. The ratio of γ/S_{e} is the coefficient B, which can be understood as the kinetic electron yield caused by the unit electronic stopping power. In the process of interaction between incident ions and target atoms, the kinetic energy of incident ions can be transferred to valence electrons and excite them, resulting in electron emission. Or the kinetic energy of the incident ions can be transferred to the inner-shell electrons, causing them to ionize and leave holes. The x-rays are generated along with the de-excitation of the holes. Here, there may be a competitive relationship in energy transfer between the inner shell electrons and the outer shell electrons.

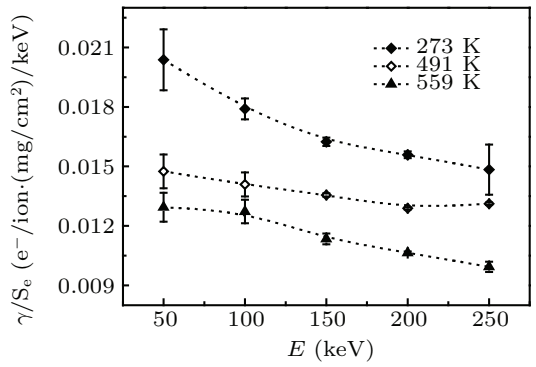


Fig. 5. ratio of kinetic electron yield γ to electronic stopping power S_{e} as a function of incident energy.

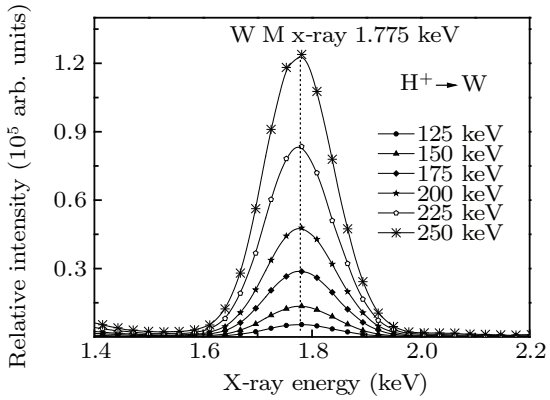


Fig. 6. Normalized tungsten x-ray spectra induced by protons impacting W target.

In order to verify the above hypothesis about the dependence of the coefficient B on the energy of protons, we measure the x-rays emitted by protons incident on W target. Figure 6 shows the typical x-ray spectra from 125-keV–250-keV protons impacting W surface (the relative intensity at the energy of 50 keV–100 keV is too small to display). We normalize the x-ray spectra by the total number of incident ions. We observe different spectral lines with the energy of about 1.775 keV and identify them with the M shell x-rays of tungsten.

The number of x-rays caused by each incident ion is defined as the x-ray yield Y. It can be calculated based on the x-ray counts obtained from the experiment.[4] The x-ray yield Y is expressed as

$$Y = N_{\mathrm{X}}/[N_{\mathrm{p}}\eta(\Omega/4\pi)], \tag{7}$$

where N_{X} is the x-ray count and obtained from the spectrum by using Gaussian fitting, N_{p} is the total number of incident ions, η is the detection efficiency of the silicon drift detector, and Ω is the solid angle of the SDD, which is 1.1 msr in our work.

Our targets can be regarded as thick targets. We can use the thick target equation to calculate the x-ray production cross section through using the measured x-ray yield and the energy loss of protons,[30]

$$\sigma_X(E) = \frac{1}{n}\frac{\mathrm{d}Y}{\mathrm{d}E}\frac{\mathrm{d}E}{\mathrm{d}R} + \frac{\mu}{n}\frac{\cos\theta}{\cos\varphi}Y(E). \tag{8}$$

Here, n is the target atomic density, $\mathrm{d}E/\mathrm{d}R$ (in units keV/cm) is the energy loss simulated by SRIM,[24] μ is the absorption coefficient of the measured characteristic x-ray, θ is the incident angle, which refers to the angle between the incident ion direction and the normal direction of the target surface, φ is the observation angle with respect to the normal direction of the target surface, $Y(E)$ is the x-ray yield per incident ion with the kinetic energy of E, $\mathrm{d}Y/\mathrm{d}E$ means the slope of the measured $Y(E)$ *versus* E, evaluated at the incident energy of E.

The M x-ray emission is closely related to the ionization cross section σ_{M} of the M shell. This ionization cross section can be obtained from the theoretical calculation of BEA and ECPSSR, and it can also be deduced from the experimental results of x-ray production cross section σ_{X},[30]

$$\sigma_{\mathrm{M}} = \sigma_{\mathrm{X}}/\omega. \tag{9}$$

Here ω is the fluorescence yield. It can be seen from Fig. 7 that the BEA theory underestimates our experimental data at the incident energy higher than 100 keV and overestimates the experimental data at the incident energy of 50 keV. It is also found that ECPSSR, which is considered to be the best theory for simulating the inner-shell ionization of light ions, is in good agreement with the experimental results within the error range. Therefore, it is suitable to use the ECPSSR theory to describe the ionization of M shell. In our results, σ_{M} is about $10^{1\sim4}$ barn (1 barn = 10^{-24} cm^2), which increases with incident proton energy increasing.

In order to further verify the ionization competition of electrons in different shells, we also explore the distribution of energy loss of incident protons between the ionization of inner electrons and the ionization of valence electrons. As mentioned earlier, the kinetic electron emission is caused mainly by the excitation of valence electrons. This process can be described as direct collisions between the light ions and the valence electrons of the target. For tungsten target, 4f, 5d, and 6s are the three outermost shells, which contribute to the electron emission. We use the BEA model theory to calculate the three values of shell ionization cross section σ_i as shown in Fig. 8. The results show that σ_i decreases to about 10^9 barn with incident energy increasing.

From Figs. 7 and 8, it can be found that the ratios of ionization cross section (σ_M and σ_i) to electronic stopping power S_e present inverse trend as a function of the proton energy. This is essentially an indirect reflection of the observations of x-ray and electron emission. It directly proves the hypothesis that there is a competition of the ionization of electrons among different shells of the target, caused by the motion of the incident ions. For a given collision, if the kinetic energy of the incident ion contributes to the ionization of the inner shell electrons, it will not lead the outer shell electrons to excite, and vice versa. In addition, σ_M is about 4–8 orders of magnitude smaller than σ_i. This also verifies that the electron emission caused by the inner-shell ionization can be ignored in our case, and the emitted electrons come mainly from the excited valence electrons.

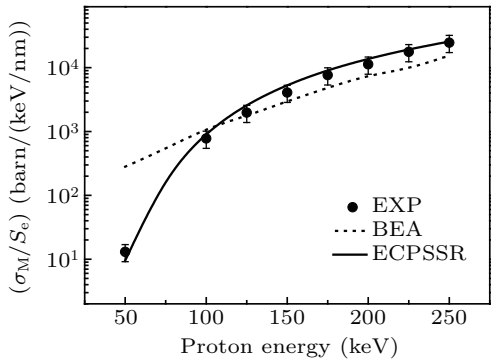


Fig. 7. Ratio of ionization cross section of tungsten inner electrons to electron stopping energy power S_e as a function of proton energy.

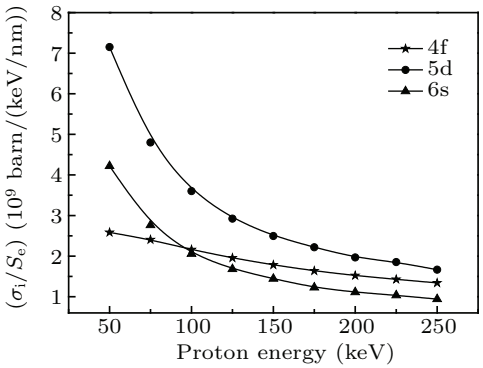


Fig. 8. Ratio of ionization cross section of tungsten valence electrons to electron stopping power S_e as a function of proton energy.

4. Conclusions

Electron emission yield from tungsten surface, induced by 50-keV–250-keV protons, has been measured at different target temperatures. We find that as the incident energy increases, the ratio of the total electron emission yield to the electronic stopping decreases. The escape of excited valence electrons is the main source of the measured kinetic electron yield. The contribution of inner shell ionization to secondary electron emission is negligible, because ionization cross section of the inn shell is about 4–8 orders of magnitude smaller than that of valence electrons. There is a competition of ionization between outer shell electrons and inner shell electrons. This leads the experimental results of electron x-ray emission to present opposite trends as a function of incident energy. Our results will provide very useful data for the study of electron emission, x-ray emission, and surface analysis of tungsten.

Acknowledgements

We are indebted to the staff of the 320-kV ECR platform and Plasma Physics at IMP for their technical support.

Project supported by the National Natural Science Foundation of China (Grant Nos. 11605147, 11375138, and 11505248), the Natural Science Basic Research Plan in Shaanxi Province, China (Grant Nos. 2019JQ-493 and 2021JQ-812), the Scientific Research Program Funded by Shaanxi Provincial Education Department, Shaanxi Province, China (Grant Nos. 20JK0975 and 16JK1824), the Shaanxi University Young Outstanding Talents Support Program, the Xianyang Normal University Young and Middle-aged Top-notch Talents Project, Shaanxi Province, China (Grant No. XSYBJ202004), and the Academic Leader Project of Xianyang Normal University, Shaanxi Province, China (Grant No. XSYXSDT202109).

References

[1] Uhm H S, Choi E H and Cho G S 2009 *Appl. Phys. Lett.* **94** 031501
[2] Hoffmann D H, Blazevic A, Korostiy S, Ni P, Pikuz S A, Rosmej O, Roth M, Tahir N A, Udrea S, Varentsov D, Weyrich K, Sharkov B Y and Maron Y 2007 *Nucl. Instr. Method Phys. Res. Sec. A* **577** 8
[3] Winter H P and Burgdörfer J 2007 *Slow Heavy-Particle Induced Electron Emission from Solid Surfaces* (Berlin, Heidelberg, New York: Springer) pp. 39–72
[4] Zhou X M, Wei J, Cheng R, Chen Y H, Mei C X, Zeng L X, Liang C H, Li Y Z, Zhao Y T and Zhang X A 2021 *Chin. Phys. B* **30** 083201
[5] Sporn M, Libiseller G, Neidhart T, Schmid M, Aumayr F, Winter HP, Varga P, Grether M, Niemann D and Stolterfoht N 1997 *Phys. Rev. Lett.* **79** 945
[6] Hayderer G, Schmid M, Varga P, Winter H P, Aumayr F, Wirtz L, Lemell C, Burgdörfer J, Hägg L and Reinhold C O 1999 *Phys. Rev. Lett.* **83** 3948
[7] Eder H, Messerschmidt W, Winter H P and Aumayr F 2000 *J. Appl. Phys.* **87** 8198
[8] Wang Y Y, Sun J R, Zhao Y T, Cheng R, Ren J R, Yu Y and Zhou X M 2013 *Nucl. Instr. Method B* **317** 33
[9] Wang X, Zhao Y T, Cheng R, Zhou X M, Xu G, Sun Y B, Lei Y, Wang Y Y, Ren J R, Yu Y, Li Y F, Zhang X A, Li Y Z, Liang C H and Xiao G Q 2012 *Phys. Lett. A* **376** 1197

[10] Winter H and Aumayr F 1999 *J. Phys. B: At., Mol. Opt. Phys.* **32** 39
[11] Xu Z F, Zeng L X, Zhao Y T, Wang J G, Wang Y Y, Zhang X A, Xiao G Q and Li F L 2012 *Laser Part. Beams* **30** 319
[12] Zeng L X, Xu Z F, Zhao Y T, Wang Y Y, Wang J G, Cheng R, Zhang X A, Ren J R, Zhou X M, Wang X, Lei Y, Li Y F, Yu Y, Liu X L, Xiao G Q and Li F L 2012 *Laser Part. Beams* **30** 707
[13] Zeng L X, Zhou X M, Cheng R, Wang X, Ren J R, Lei Y, Ma L D, Zhao Y T, Zhang X A and Xu Z F 2017 *Sci. Rep.* **7** 6482
[14] Hughes I G, Folkerts L, Folkerts L, *et al.* 1993 *Phys. Rev. Lett.* **71** 291
[15] Vana M, Kurz H, Winter H P and Aumayr F 1995 *Nucl. Instr. Method B* **100** 402
[16] Mcguire J H and Richard P 1973 *Phys. Rev. A* **8** 1374
[17] Johnson D E, Basbas G and Mcdaniel F D 1979 *At. Data Nucl. Data Tables* **24** 1
[18] Lapicki G and Mcdaniel F D 1980 *Phys. Rev. A* **22** 1896
[19] Miranda J and Lapicki G 2014 *At. Data Nucl. Data Tables* **100** 651
[20] Zhou X M, Zeng L X, Cheng R, Lei Y, Chen Y H, Xu Z F, Chen X M, Wang Y Y, Zhao Y T and Xiao G Q 2017 *Nucl. Instr. Method B* **406** 491
[21] Zhao Y T, Xiao G Q, Xu H S, Zhao H W, Xia J W, Jin G M, Ma X W, Liu Y, Yang Z H, Zhang P M, Wang Y Y, Li D H, Zhao H Y, Zhan W L, Xu Z F, Zhao D, Li F L and Chen X M 2009 *Nucl. Instr. Method B* **267** 163
[22] Zhang X A, Zhao Y T, Hoffmann D H, Yang Z H, Chen X M, Xu Z F, Li F L and Xiao G Q 2011 *Laser Part. Beams* **29** 265
[23] Ewing R I 1965 *Phys. Rev.* **139** 1840
[24] http://www.srim.org/SRIM/SRIM2011.htm
[25] Hölzl J and Schulte F K 1979 *Springer Tr. in Mod. Phys.* (*Solid State Phys.*) **85** 1
[26] Stoöck J, Suta T, Ditroi F, Winter H P and Aumayr F 2004 *Phys. Rev. Lett.* **93** 263201
[27] Kishinevsky L M 1973 *Radiat. Effects* **19** 23
[28] Ritzau S M and Baragiola R A 1998 *Phys. Rev. B* **58** 2529
[29] Zhao Y T, Xiao G Q, Xu Z F, Qayyum A, Wang Y Y, Zhang X A, Li F L and Zhan W L 2007 *Acta Phys. Sin.* **56** 5734 (in Chinese)
[30] Garcia J D, Fortner R J and Kavanagh T M 1970 *Rev. Mod. Phys.* **45** 111